



TITLE:

Sedimentary features observed in the tsunami deposits at Rikuzentakata City

AUTHOR(S):

Naruse, Hajime; Arai, Kazuno; Matsumoto, Dan; Takahashi, Hiroki; Yamashita, Shota; Tanaka, Gengo; Murayama, Masafumi

CITATION:

Naruse, Hajime ...[et al]. Sedimentary features observed in the tsunami deposits at Rikuzentakata City. *Sedimentary Geology* 2012, 282: 199-215

ISSUE DATE:

2012-12

URL:

<http://hdl.handle.net/2433/166602>

RIGHT:

© 2012 Elsevier B.V.; この論文は出版社版ではありません。引用の際には出版社版をご確認ご利用ください。; This is not the published version. Please cite only the published version.

1 Sedimentary features observed in the tsunami deposits at Rikuzentakata City

Hajime Naruse^{1*}, Kazuno Arai², Dan Matsumoto³, Hiroki Takahashi², Shota Yamashita²,
Gengo Tanaka⁴, and Masafumi Murayama⁵

¹Kyoto University, Division of Earth and Planetary Sciences, Graduate School of Science, Kitashirakawa-Oiwakecho, Sakyo-ku, Kyoto 606-8502, Japan

²Chiba University, Division of Earth Sciences, Graduate School of Science, 1-33 Yayoicho, Inage-ku, Chiba 263-8522, Japan

³Advanced Industrial Science and Technology, Institute of Geology and Geoinformation, 1-1-1 Higashi, Tsukuba, Ibaraki 305-8561, Japan

⁴Gunma Museum of Natural History, 1674-1, Kamikuroiwa, Tomioka-shi, Gunma 370-2345, Japan

⁵Kochi University, Center for Advanced Marine Core Research, B200 Monobe, Nankoku, Kochi 783-8502, Japan

*Corresponding author: naruse@kueps.kyoto-u.ac.jp Fax: +81-75-753-4189

2

3

Abstract

4 The March 11, 2011 Tohoku-Oki tsunami triggered by an earthquake off the
5 east coast of northeastern Honshu Island (Tohoku region), Japan, deposited large
6 amounts of sediment on land, including the Sendai Plain and Sanriku Coast. This study
7 reports on the characteristics of the tsunami deposits in Rikuzentakata City, southeastern
8 Iwate Prefecture, northeastern Japan. A field survey identified the inundation pattern of
9 the tsunami in this region and the facies model of the tsunami deposits at the bay-head
10 deltas of estuarine systems. The tsunami deposits in Rikuzentakata City generally
11 consist of one to four units that represent a discrete runup or backwash flow. Each unit
12 is characterized by initial inverse grading and successive normal grading that
13 correspond to the accelerating and decelerating stages of the flow, respectively. An
14 internal erosional surface often developed between the inverse-graded and
15 normal-graded units. It corresponds to the maximum shear velocity of the flow and
16 truncates the underlying inverse-graded unit. In the case of the runup unit, silty
17 fine-grained drapes overlay the graded sandy interval. A correlation of the sedimentary
18 structures and grain fabric analysis revealed that the Tohoku-Oki tsunami inundated
19 Rikuzentakata City at least twice and that the flow velocity exceeded 2.4 m/s.
20 Paleontological analysis of the sediment and kriging estimation of the total volume of
21 the tsunami deposit implied that the sediments were sourced not only from eroded beach
22 sands but also from the seafloor of Hirota Bay or more offshore regions.

23 KEYWORDS: tsunami; inverse-graded bedding; graded bedding; Northwest Pacific;

24 ostracods

25

1. Introduction

The Tohoku-Oki tsunami was triggered by an earthquake that occurred at 14:46 on March 11, 2011, with the epicenter located off the east coast of northeastern Honshu Island (Tohoku region), Japan (Fig. 1). The Mw 9.0 earthquake is the largest recorded event in Japan (Fujii et al., 2011) and the fourth-largest in the last 100 years in the World (Nettles et al., 2011). According to the Japan Meteorological Agency, the earthquake resulted from a series of seismogenic faulting events that began at 38.1035°N, 142.861°E, Mw 9.0 at 14:46:18 JST, along the Japan Trench, where the Pacific Plate is subducting beneath the North American Plate. The resulting tsunami spread across the North Pacific Ocean (Stimpson, 2011), striking coastal areas of Japan with a maximum run-up height of 39.7 m in Miyako city, Japan (Mori et al., 2011). As of 8 August, 2012 (National Policy Agency of Japan, 2012), the estimated fatalities were 15,868 with 2,848 persons still missing.

The tsunami inundation caused severe damage, especially in the coastal regions of northeastern Japan, such as Fukushima, Miyagi, and Iwate Prefectures. This study reports on the characteristic features of the tsunami deposits in Rikuzentakata City, southeastern Iwate Prefecture, northeastern Japan (Figs. 1 and 2). The city suffered catastrophic destruction (Figs. 3 and 4) with an estimated 1,552 fatalities and an additional 399 persons missing as of July 14, 2011 (<http://sv032.office.pref.iwate.jp/~bousai/>). This is the largest number of fatalities in Iwate Prefecture. The city remains at risk from future tsunamis, as do other areas with similar topographic features, thus it is important to understand the behavior of tsunami

waves in this region for future disaster mitigation. Another significance of the research in this region is that a field survey in Rikuzentakata City may potentially reveal features of tsunami deposition in natural environments without the influence of artificial infrastructure. Most cities on the Sanriku Coast were protected by artificial coastal levees, aiming at trapping most of the sediment transported by tsunami waves. Hence, less deposition is expected than in the case of ancient tsunami deposits. In the case of Rikuzentakata City, however, the first tsunami wave completely destroyed a 5.5-m-high coastal levee, resulting in large-scale erosion of the sandy coast (Fig. 3). This coastal erosion provided abundant source sediments that were deposited on land, forming a thick and extensive tsunami deposit. Therefore, it is expected that the facies model of the tsunami deposits in this region may be comparable to ancient events and will be helpful in deciphering geological records. There are also extensive studies of the 2011 Tohoku-Oki tsunami deposits on the Sendai Plain (e.g. Goto et al., 2011; submitted this issue; Abe et al., in press this issue), and therefore the future comparison of results between the Sanriku Coast and Sendai Plain regions will be significant, focusing on influences of topographic settings on the sedimentary features of tsunami deposits.

This study aims to contribute to future research on tsunami deposits and disaster prevention from two viewpoints: (1) providing information about the behavior of the Tohoku-Oki tsunami in this region and (2) establishing a facies model of the tsunami deposits at the bay-head deltas of estuarine systems. Terrestrial tsunami deposits provide important information on the magnitude and recurrence intervals of tsunami events (Nanayama et al., 2003). Reconstruction of the hydraulic properties and magnitude of historical tsunamis from stratigraphic sequences can be useful in risk assessment studies. However, sandy beds in coastal stratigraphic successions may also

be produced by events such as large-scale storms and river flooding (e.g., Switzer & Jones, 2008). Therefore, it is important to investigate the detailed features of recent tsunami deposits from known source events because their sedimentological characterization and relationship with the actual events are necessary for establishing the criteria to identify tsunami deposits in the geological record.

Documentation of the Tohoku-Oki tsunami is also significant for the verification and improvement of numerical tsunami models, which will be important for future disaster-prevention measures. Direct measurements of flow velocities or hydrographs of the tsunami are not available for this region; hence, an investigation of the deposits is useful in providing information on this hazard. From this viewpoint, the study examined the number of inundations, estimated minimum flow velocities, and calculated the total flux of tsunami sediment. These characteristics will be reproduced in future studies by numerical models with sediment transport functions.

2. Study Region

Rikuzentakata City, on the southern Sanriku Coast, is approximately 130 km west of the earthquake epicenter (Fig. 1). The central–southern part of the Sanriku Coast is a mountainous region with a deeply indented Ria coastline, which features a series of alternating capes and estuaries, with small bay-head deltas often developed at the river mouths.

Rikuzentakata City is located in an estuarine bay-head delta plain in the inner part of Hirota Bay (Fig. 1 and 2). The coastal delta plain is approximately 2 km wide in the north–south direction and extends for 2.5 km east–west. Most regions of the

94 delta-plain are relatively flat and are less than 5 m above mean sea level. This delta
95 plain was formed by the 50 km long Kesen River, which has a drainage basin area of
96 540 km². Progradation of the delta was initiated approximately 6000 years before
97 present in response to Holocene sea level rise, and the modern delta plain was mostly
98 established by about 3000 years before present (Chida et al., 1984). The most prominent
99 topographic feature of Rikuzentakata City was the Takata-Matsubara pine forest, located
100 on a wave-dominated spit (Fig. 3) on top of which a 5.5-m-high coastal levee had been
101 built (Asano et al., 2009).

102 The maximum tsunami run-up height was 19.9 m in this region, and the
103 inundation height (tsunami height above mean sea level) was approximately 14–15 m
104 (reported by The 2011 Tohoku Earthquake Tsunami Joint Survey Group at
105 <http://www.coastal.jp/tjt/>). The exact number of inundations and periodicity of the
106 tsunami waves at Rikuzentakata City is unknown because all tidal gauges and global
107 positioning system (GPS) buoys in this area were destroyed by the event. However, data
108 from a GPS buoy located off southern Iwate Prefecture (39.3361°N, 141.9944°E), ca. 15
109 km offshore, indicate that seven successive waves struck this coast (Takahashi et al.,
110 2011). The first wave was the largest (6.7 m in height at this site), the second and fourth
111 waves were relatively high (approximately 2 m in height), and others were relatively
112 small (less than 1.5 m in height). The wave periodicity was approximately 50 min
113 (Takahashi et al., 2011). Numerical simulation suggests that the tsunami showed a
114 similar wave pattern close to Rikuzentakata City (Fujii et al., 2011). However, the
115 complicated shape of the Sanriku coastline influences wave height and periodicity near
116 the coast and so tsunami waves inundating the coast cannot be expected to precisely
117 follow the patterns indicated by these offshore data.

The 2011 Tohoku-Oki tsunami largely eroded the spit in this region, transporting a large amount of sandy sediments on land. Takata-Matsubara was artificially designed to prevent storm and tsunami disasters, and had previously resisted two major tsunamis, the 1896 Meiji Sanriku Tsunami and the 1933 Showa Sanriku Tsunami (Asano et al., 2009). However, the forest was completely destroyed by the 2011 Tohoku-Oki tsunami and only one pine tree survived, indicating the intensity of the event. Tsunami waves easily spilled over and destroyed the levee behind Takata-Matsubara (Figs. 3 and 4). As a result, most of the city was inundated to a distance of more than 2 km from the shoreline, covering an area of 13 km² from the map provided by Geospatial Information Authority of Japan and the analysis by the Tsunami Damage Mapping Team, Association of Japanese Geographers (http://danso.env.nagoya-u.ac.jp/20110311/map/index_e.html; Fig. 2).

3. Methodology

We surveyed the topographic features (erosional structures and bedforms) of tsunami inundation and investigated sedimentary features of the tsunami deposits by visual observation, grain-size and fabric analysis. Micropaleontological analysis was also conducted to help estimate sediment sources.

3.1 Field Survey

We conducted approximately one week of fieldwork in Rikuzentakata City between April 24–26 and June 10–12, 2011. The inundated region of Rikuzentakata City can be subdivided into the main city and the Otomo area, a small settlement a few

km from the main town and located on flat land at the end of Hirota Peninsula (Fig. 2). Our survey covered both inundated regions, mostly focusing on areas that were originally rice fields. While buildings and artificial structures have complex effects on tsunami waves, the rice fields are flat and are therefore expected to display the primary features of tsunami deposition without artificial influences. The alignment of felled power poles and crests of bedforms (dunes) were measured to estimate the flow directions of tsunami waves (Fig. 4 and 5).

Study site locations were established using a GPS. For each observation site, we examined the erosional features and the distribution of tsunami sediments and excavated pits to measure the sediment thickness and depositional structures.

Bulk sediment samples for grain-size and micropaleontological analysis were also taken from each sampling pit. At several locations where the tsunami deposits were relatively thick (~10 cm), trenches several meters long and 10 to 40 cm deep were excavated, and the trench walls were peeled off onto cloth by using polyurethane resin (Fig. 6), in order to examine details of the sedimentary structures and conduct grain-fabric analysis.

3.2 Grain-size Analysis

Grain-size distributions of tsunami deposits were analyzed using a Mastersizer 2000 laser granulometer (Malvern Instruments, Malvern, UK). Before analysis, the organic matter was removed using hydrogen peroxide, and sieving was performed to separate sediments coarser than 2 mm. Samples were then treated with sodium hexametaphosphate as dispersant to scatter the fine sediments (Sperazza et al., 2004). We converted the measured grain sizes to the phi scale ($\phi = -\log_2 D$ where D is the

particle diameter in mm). Mean grain size $\bar{\phi}$, sorting s , skewness S_k , and kurtosis K_t were calculated on the basis of the moment method (Folk, 1966; Harrington, 1967), as follows:

$$\bar{\phi} = \frac{\sum p\phi_i}{100} \quad (1)$$

$$s = \sqrt{\frac{\sum p(\phi_i - \bar{\phi})^2}{100}} \quad (2)$$

$$S_k = \frac{\sum p(\phi_i - \bar{\phi})^3}{100s^3} \quad (3)$$

$$K_t = \frac{\sum p(\phi_i - \bar{\phi})^4}{100s^4} \quad (4)$$

where ϕ_i is a representative value of each grain-size class (every 0.17 phi), and p is a weight fraction (in percentage) for each grain-size class. The 10th, 50th, and 90th percentile grain-size values D_{10} , D_{50} and D_{90} respectively, were also provided for each sample.

We measured gravels directly with a caliper and described the length of their b-axes as a representative diameter for the computation of the critical flow velocity, which is described in section 3.3.

3.3 Critical Flow Velocity of Particle Motion

The minimum estimation of the flow velocity of the tsunami wave was derived from grain-size analysis and the size of the largest particles (>2 mm in b-axis diameter) on the basis of the critical shear stress of initiation of particle motion with consideration of mixed grain-size effect. Here, the hydraulics of oscillatory flows caused by the waves are approximated by using uni-directional open-channel flows because the periodicity of tsunami waves is sufficiently long to justify this approximation. Indeed, the GPS buoy

measurement suggested that the periodicity of the Tohoku-Oki tsunami near Rikuzentakata City was approximately 50 min (Takahashi et al., 2011). Therefore, critical Shields values τ_c^* can be regarded as those commonly used to denote conditions under which bed sediment particles are stable but on the verge of being entrained in open-channel flows. A fit to the Shields data by Brownlie (1981) with modification proposed by Neil and Yalin (1969) is as follows (Garcia, 2008):

$$\tau_c^* = 0.11 Re_p^{-0.6} + 0.03 \exp(-17.77 Re_p^{-0.6}) \quad (5)$$

where Re_p is the particle Reynolds number, defined as $Re_p = \sqrt{RgD}D/\nu$ (R : submerged specific density of sediments (1.65), g : acceleration due to gravity (9.81 m/s²), D : sediment diameter, and ν : kinematic viscosity of ambient fluid), and where the dimensionless Shields shear stress is defined as follows:

$$\tau^* = \frac{u_*^2}{RgD} \quad (6)$$

Here, u_* denotes shear velocity. Thus, the critical Shields shear stress τ_{c50}^* for particles of median grain-size D_{50} can be calculated by equation 5. However, mixed-size grains do not act the same as when they are surrounded by grains of the same size (Einstein, 1950), and the coarser grains exposed on the surface protrude more into the flow, resulting in a preferentially greater drag. This exposure effect (hiding effect) can be corrected by considering a power-law relationship:

$$\frac{\tau_{ci}^*}{\tau_{c50}^*} = \left(\frac{D_i}{D_{50}} \right)^{-\gamma} \quad (7)$$

where γ is an empirical parameter that varies from 0.0 to 1.0 (Parker, 2005). From equations 6 and 7, the critical depth-averaged flow velocity $U_{c \max}$ of the largest grain

(diameter is D_{\max}) in the tsunami deposit can be calculated from the following equation:

$$U_{c\max} = C_f^{-\frac{1}{2}} \sqrt{RgD_{\max} \left(\frac{D_{\max}}{D_{50}} \right)^{-\gamma} \tau_{c50}^*} \quad (8)$$

Here, C_f is a friction coefficient of uni-directional open-channel flows, defined as follows:

$$U_{c\max} = C_f^{-\frac{1}{2}} u_{*c\max} \quad (9)$$

To estimate the critical flow velocity of initiation of particle motion, two empirical parameters, γ and C_f , must be determined. The value of γ generally ranges from 0.65 to 0.90 (Parker, 2005), and becomes zero in the case of very large grains (Ramette and Heuzel, 1962); hence, we considered the value zero when estimating the flow velocity of the tsunami wave from the largest grain in the deposit. On the other hand, for hydraulically rough flows, the friction coefficient C_f is given by the following equation:

$$C_f = \left[\frac{1}{\kappa} \ln \left(11 \frac{H}{k_s} \right) \right]^{-2} \quad (10)$$

where κ is the Karman constant (~ 0.4); H , the flow thickness; and k_s , the effective roughness height (Keulegan, 1938). k_s is empirically considered to be proportional to a representative sediment size D_{90} , such that the following relationship holds:

$$k_s = \alpha D_{90} \quad (11)$$

The suggested value of α is 3.0 (Van Rijn, 1982). It is difficult to precisely estimate the flow height of the tsunami wave during deposition of the bed in which the particles of the maximum grain-size occurred, so we tentatively set the flow height as 10–15 m.

The critical flow velocity required to transport the maximum grain-size observed at each site can be estimated using equations 5, 8, 10, and 11. The estimated velocity is, however, the minimum requirement for the tsunami waves that hit Rikuzentakata City. As suggested by Hiscott (1994), the actual flow velocity could far exceed the critical flow velocity of particle motion.

3.4 Grain Fabric Analysis

The grain fabric of vertical sections of sandy tsunami deposits was examined to analyze the paleocurrent of the oscillatory flows. Trenches were excavated at several localities parallel to the direction of the paleoflow which was estimated by the bedform, and a peel of the trench wall was obtained using polyurethane resin and a mesh. High-resolution images of the peeled sample were captured using a digital camera at 4800 dpi. All the grains identified in the images were traced manually, and then each traced grain was approximated by an ellipse, using the public-domain ImageJ program (<http://rsb.info.nih.gov/ij/>). The locations and elongation directions of the grains were obtained as quantitative image-analysis data. The location was taken as the average of the x and y coordinates of pixels included in the traced grain, and the elongation direction was obtained as the angle between the primary axis of an ellipse fitted to the grain by the Hough transform and the line parallel to the x axis of the image. All measured data are considered to be the apparent two-dimensional characteristics of three-dimensional features. The present study therefore examines only the apparent features of the tsunami deposit samples, assuming equivalence to the three-dimensional structure.

3.5 Micropaleontology

In order to determine the sediment source, we investigated ostracods included in the onshore tsunami deposits formed by the Tohoku-Oki tsunami. Ostracods are small crustacea (0.3–30 mm long) with calcified valves adapted to practically every aquatic environment. Thus, fossilized valves are an important paleoenvironmental indicator, particularly with regard to Holocene oceanographic, climatologic, and geologic events (Nelson et al., 2008). Marine podocopid ostracods are exclusively benthic crustaceans that are abundant in marine sediments. Furthermore, most species show regional endemism, and hence, they can be an important indicator of local bottom-water environments. The valves behave like sediment grains in the water column. We collected ostracod specimens by sieving and manual picking, and then used the modern analog technique (MAT) to infer paleoenvironmental conditions by comparing fossil ostracod assemblages in the onshore sediments with similar assemblages in the modern environment (Ikeya and Cronin, 1993). We compared Holocene ostracod assemblages sampled from 476 surface sediments of the seafloor around Japan with those recovered from sediments deposited by the tsunami, approximately 4 km southeast of Rikuzentakata City (Fig. 2).

3.6 Spatial Interpolation of Measured Data

The kriging method was employed to estimate the spatial variations in mean grain-size and thickness parameters (Burgess and Webster, 1980a,b; Kohsaka, 1998). Kriging is an algorithm based on least-squares and is used to estimate the spatial variation in a real-valued function; it is based on the assumption that the spatial variation can be estimated from a linear combination of measured values (Kohsaka,

1998). Weighting coefficients are obtained on the basis of the spatial dependence of a variable; this can be represented by a semivariogram, i.e., the scatter diagram of covariance with respect to spatial distance. The weighting of the running average is then determined by the variogram model function, which is the fitted function to the semivariogram (Burgess and Webster, 1980a). Theoretically, the covariance of spatial data increases with distance and becomes a steady value at distances exceeding a particular threshold (Burgess and Webster, 1980a,b; Kohsaka, 1998). This limited distance is the range within which the data indicates spatial dependence. The spatial dependencies of the data are also shown in the estimation variances, which provide a measure of the uncertainty in the interpolation values. When directional anisotropy was detected in semivariograms, geometric anisotropy was removed by applying an affine transformation to the distances of the sample sites.

Spatial distributions of deposition thickness and mean grain-size data were interpolated across the entire surveyed region. Semivariograms were calculated from the measured data, and variogram models were fitted using the weighted least-squares method. Both the interpolated values and estimation standard errors were shown as color images.

4. Results

4.1 Topographic Features and Bedforms

In regions up to approximately 500 m from the shoreline, erosion by the tsunami dominated where flute-like depressions with erosional fringes were observed

(Fig. 4C), ranging in diameter from 10 cm to several meters. Deformed sedimentary features or upward injection of sands that are generally associated with liquefaction were not observed. Although detailed topographic measurements were not conducted, the severe erosion that removed the pine forest on the spit appeared to extend to a depth of around 0.5 to 1 m. Analysis of aerial photographs (Fig. 3) indicated that the region eroded by the tsunami was approximately $3.5 \times 10^5 \text{ m}^2$.

All power poles observed in Rikuzentakata City were bent by tsunami inundation flows (Fig.4B), and the orientation of the fallen poles indicated that the flooding direction was mostly northward within the main city area, whereas several poles in the main city also indicate southward backwash currents (Fig. 7).

Tsunami deposits were distributed across the entire inundated area of Rikuzentakata City (Figs. 5 and 6). In most areas, a uniform thickness generally draped the natural topography. However, dunes were occasionally formed by flooding or backwash currents in both the main city and the Otomo areas (Fig. 5A). Dunes are composed of coarse sand and pebbles, with wavelengths generally ranging from 1 to 10 m. The largest dune was composed of cobble-sized gravels and was observed in the Otomo area (Fig. 5A); it had a wavelength of 10 m and was 30–40 cm high. Flow directions suggested by dune crests and foresets were southwestward (N230°) in the main city area, and southeastward (N144°) in the Otomo area.

4.2 Thickness Variation

The field survey and kriging interpolation helped determine the thickness of the tsunami deposits in Rikuzentakata City (Fig. 8). The transported sediment started to be laid down approximately 500 m from the shoreline, and attained a maximum thickness

(31.5 cm) within the next 100 m. The thickness of the deposits then gradually decreased landward; however, local variations in sediment thickness were observed in relation to topographic depressions or elevations. The tsunami deposits continued to the maximum extent of inundation, where the thickness of muddy deposits ranged from 0.5 to 2 cm (Fig. 8; Table 2).

As the tsunami deposits varied in thickness throughout Rikuzentakata City, the total deposition was calculated by summing the interpolated distribution, giving an estimate of $6.1 \times 10^5 \text{ m}^3$ transported material (standard error $1.5 \times 10^3 \text{ m}^3$).

4.3 Sedimentary Structures and Units

Based on observation of sedimentary structures in pits and trenches, it was determined that the tsunami deposits in Rikuzentakata City were composed of one to four sedimentary units, identified by distinctive sedimentary structures and grain-size changes (Figs. 9, 10 and 11). Each sedimentary unit ranged from 1 to 10 cm in thickness, and showed a flat, layer-like geometry (Figs. 6, 9, 10 and 11). Each unit typically consisted of inverse-graded sand overlain by normally graded or gravelly sand (Fig. 9). The normally graded sub-unit was generally thicker than the inverse-graded one. The boundary between these two sub-units was often a sharp erosional surface, and occasionally the inverse-graded sub-unit was truncated. A thin mud drape (<1 cm) occurred on the top of the normally graded division (Fig. 9). Each unit commonly showed parallel lamination and, less frequently, current ripple cross-lamination could be observed (Fig. 9). The lowermost unit was generally the thickest and coarsest, and often contained large clasts, such as pebbles or cobbles, within sands (Fig. 10). The upper units showed upward thinning and fining, and large clasts were rare in these units.

Each unit in the deposit showed evidence that it was formed under a unidirectional runup or backwash current of the tsunami wave (Fig. 11). Grain fabric analysis indicated that the flow direction was constant within an inverse-graded to graded unit and varied from runup to the backwash current at the boundary between units (Fig. 12). The paleocurrent direction shown by cross-lamination and dunes is consistent with the grain-fabric data (Figs. 10, 11 and 12).

The thickness and number of units in the deposits decreased landward, and the sandy sub-unit finally disappeared near the edge of tsunami inundation (Fig. 10 and 11), although mud drapes were continuous. Flow-parallel variations in the thickness and sedimentary structures of units were examined at two transects, one is in the eastern region of the main city area (Transect 1) and another is in the Otomo area (Transect 2) (Fig. 11). In Transect 1, the tsunami deposit was composed of two inverse-graded to normally graded units at the seaward end (Fig. 11). The lower unit was a 15-cm-thick very coarse pebbly sand, and showed thinning and fining landward. The upper unit was a 5-cm-thick medium sand, which pinched out within 500 m. In Transect 2, three units occurred at the upstream end of the runup current (Fig. 11). Grain-fabric analysis and cross-lamination suggest that the first and third units were formed by the southeastward runup current (Fig. 12), and that the second unit was formed by the northwestward backwash current. The first unit was thick and was the coarsest, containing shell fragments at its top. This unit showed fining and thinning down current, but continued until the downstream end. The second unit was also thick, but pinched out within approximately 500 m. The third unit was relatively thin and showed fining and thinning down current.

4.4 Spatial Variation in Grain Size and Critical Flow Velocity for Particle Motion

Analysis of spatial variation in grain sizes indicated landward fining (Fig. 13; Table 2). Since the granulometric properties of the tsunami deposits vary vertically, we plotted data obtained from the lowermost, coarsest unit in each site (Fig. 13). The interpolated data of mean grain-size reveal that the center of the main city area was covered by sandy deposits (Fig. 13), whereas samples taken from the northern end of the inundation area were composed of muddy sediments. Thus, sand-sized sediments diminished before the limit of the inundation area. Kriging interpolation of spatial variation of mean grain-size suggests that the muddy sediments were transported 2 km further than the distribution limit of the sandy deposits (Fig. 13).

Analysis of the critical flow velocity of the largest particles revealed that the first flood wave exceeded 2.4 m/s at minimum (Fig. 14). A total of 21 sites were examined, where gravels occurred in the lowermost unit of the tsunami deposit; the estimated critical flow velocity ranged from 0.9 to 2.4 m/s when the flow height was set to 10 m. The critical flow velocity ranged from 0.9 to 2.7 m/s when the flow height was set to the estimated maximum inundation height of 15 m. Higher critical flow velocity (2.4 or 2.7 m/s) was detected in the middle of the inundation area, slowing towards the margins (0.9 m/s; Fig. 14).

4.5 Ostracods

The ostracod assemblages were recovered from sediments deposited by the tsunami in the main city and Otomo area (collected at Locs. 19, 60, 94, 95 and 96 of Fig. 2 on April 25; Fig. 15 and Table 1). A sample taken at Loc. 60 contained abundant

ostracod specimens, and was characterized by inner bay species, such as *Bicornucythere bisanensis* (Fig. 15B-1), *Nipponocythere bicarinata* (Fig. 15B-2), *Spinileberis quadriaculeata* (Fig. 15B-3), and *Cytheromorpha acupunctata* (Fig. 15B-4). It also contained some rocky shore species (*Aurila corniculata*, *Xestoleberis hanaii*) (Table 1). Some of the ostracod valves of the sample were well preserved (Figs. 15B) and translucent. Moreover, the soft parts were preserved in one *B. bisanensis* specimen (Fig. 15B-1). However, many of the ostracod valves were opaque and fragmented, indicating that the ostracod assemblage in the sample was probably derived from a thanatocoenosis on the seafloor. Thus, it was appropriate to use MAT to compare the assemblage of the sample at Loc. 60 with Holocene ostracod thanatocoenoses such as those obtained from around Japan.

By applying MAT, we determined that the ostracod assemblage in the sample of Loc. 60 was most similar to that of sample OK 28 from Osaka Bay; which had been collected from a water depth of 9 m (Fig. 15A).

5. Discussion

5.1 Use of the Tsunami Deposits in Rikuzentakata City for the Identification of Older Events

This study revealed that the tsunami deposits in Rikuzentakata City generally consisted of multiple units that represented a discrete runup or backwash flow, as described in Section 5.3 (Figs. 10, 11 and 16). Thus, for example, two inundations produced four units (two runup and two backwash). This feature of the tsunami deposit

is quite different from that on the Sendai Plain, where multiple units were not obvious (Goto et al., 2011). This difference could be attributed to differences in the tsunami hydrographs and local topography.

Each unit was characterized by initial inverse grading and successive normal grading that correspond to the accelerating and decelerating stages of the runup or backwash flow respectively (Fig. 16). Multiple units with inverse- to normal-grading were also reported from the 2004 Indian Ocean Tsunami deposits in Thailand (Naruse et al., 2010) and other coastal environments (e.g., Kon'no, 1961; Shi et al., 1995; Benson et al., 1997; Dawson & Smith, 2000; Gelfenbaum & Jaffe, 2003; Moore et al., 2006; Nanayama & Shigeno, 2006), suggesting the general applicability of this facies model of the multiple-bedded terrestrial tsunami deposits described here. Each unit of multilayered tsunami deposits have often been attributed to a discrete wave (e.g., Kon'no, 1961; Clague et al., 2000) or one set of runup/backwash currents of a tsunami (e.g., Moore & Moore, 1984; Nishimura & Miyaji, 1995; Nanayama & Shigeno, 2006). Sedimentary features within multiple-bedded tsunami deposits are often complicated (e.g., Moore et al., 2006) and their formative processes have been interpreted to be a consequence of the multiple waves of tsunamis (e.g., Fujiwara, 2007). A characteristic feature of tsunamis is the turnover of unidirectional current due to long wave period (several minutes to tens of minutes) that involves acceleration, deceleration and turnover stages.

The runup units are generally thicker than the backwash units probably because of the asymmetric behavior of tsunami waves and the availability of source sediments (Naruse et al., 2010). The tsunami waves run up with relatively uniform flow directions, whereas those of the backwash currents are generally concentrated and localized

(Umitsu, 2006; Dodd et al., 2008). This asymmetric behavior of tsunami waves is commonly observed in various environments (Umitsu, 2006; Naruse et al., 2010), and can explain the fact that backwash units in the onshore tsunami deposit are often absent or distributed only locally.

The importance of understanding the internal subunits of each unit in a tsunami deposits is critical for the identification of the runup unit. Naruse et al. (2010) proposed a facies model of tsunami deposits in which the basal inverse graded divisions (subunit I) are produced during the waxing stage of the tsunami runup or backwash flows but they are easily lost due to subsequent erosion (Fig. 16). An internal erosion surface (IES) often develops between the inverse and normal graded subunits. As a result, tsunami deposits are generally composed of graded units (subunit G) that are deposited in the waning stage of flow and therefore have a greater preservation potential. In the case of the runup flow, the stagnant stage of the tsunami wave forms silty mud drapes (subunit S). Thus, it was suggested that the sequence ideally containing units I-G-S corresponds to the runup flow and the sequence containing units I-G corresponds to the backwash flow although there are large variations due to local erosion and deposition (Fig. 16). The model assumes that deposition and erosion by tsunami waves are mostly caused by spatial differences in the rate of sediment transport, and the sites of deposition and erosion show a patchy distribution when the flow velocity field is remarkably non-uniform. Thus, remarkable lateral variations in sedimentary structures in a tsunami deposit can mostly be explained by localized erosional and depositional processes.

Without this subunit I-G-S model (Naruse et al., 2010), the flow units in a tsunami deposit may be misinterpreted. For example, the tsunami deposit in Loc. 93

appeared to be composed of 5–6 subunits that were bounded by mud drapes or erosional surfaces (Fig. 16), but the grain-fabric analysis suggested that the deposit actually consisted of three flow-units (2 runup and 1 backwash units) (Fig. 11 and 12). Erosional surfaces are intercalated within a flow unit due to the waxing of the runup or backwash flow, and the true unit boundaries are between the normal- and inverse-graded subunits (subunits G to I) or silty mud drapes (subunit S).

The trends of landward fining and thinning of each unit and a decrease in the number of units are also common features in various terrestrial environments (e.g., Fujino et al., 2010). The landward fining trend of each unit that differentiates the run-up limit of the sandy and muddy sediments is an especially significant feature for reconstructing inundation areas based on the distribution of ancient tsunami deposits. Sandy tsunami deposits were distributed widely in the main city area, whereas muddy deposits ($<4\phi$ on average) occurred near the margins of the inundation area (Fig. 13). Kriging interpolation of the mean grain-size of the deposits revealed that the tsunami can extend more than 2 km from the run-up limit of the sandy deposits (Fig. 13). Therefore, it is suggested that precise reconstruction of tsunami inundation from geological record requires the identification of muddy tsunami deposits (Goto et al., 2011). While these may be quite difficult to distinguish from surrounding soils, Chagué-Goff et al. (in press this issue) show that geochemical markers can successfully differentiate between fine grained sediments of marine or terrestrial origin. It should also be noted that the number of data control points is small in the northern region of the study area so that the result of the Kriging method is similar to that of linear interpolation. Thus, future analysis with a larger number of data control points is needed to confirm the actual transition point between sandy and muddy tsunami deposits. In our

area, the number of internal sedimentary units also decreased landward as a result of landward thinning of each unit. It is therefore recommended that the seaward end of a tsunami deposit should be studied when attempting to estimate the number of waves associated with inundation.

5.2 Reconstruction of Behavior of the Tohoku-Oki tsunami in Rikuzentakata City

The behavior of the Tohoku-Oki tsunami in Rikuzentakata City reconstructed from the analysis of tsunami deposits reveals that at least two waves inundated the city with velocities exceeding 2.4 m/s. This estimation provides minimum value of the flow velocity, and future study with evidence such as video footage or eye-witness accounts will reveal the merits and limitations of this analysis of the wave properties from the sediments. The analysis of the sediment flux and micropaleontological evidence suggests that erosion of the seafloor of Hirota Bay may have occurred and the resulting sediments probably transported on land.

In Transects 1 and 2, the basal, flooding flow, unit could be traced to the landward end of both transects (Fig. 11). The first backwash flow unit occurred in the seaward half of Transects 2, and pinched out near its center. The second runup flow unit was also continuous in Transect 2, whereas it was no longer visible in the center of Transect 1. Although the correlation between the sedimentary units in the main city area was difficult due to the complexity of sedimentary units, a maximum of four runup units could be recognized, suggesting that two or more waves also inundated this region. As described above, data from a GPS buoy located approximately 15 km offshore indicates that seven successive waves hit this coast (Takahashi et al., 2011), and that the first

wave was the largest. The first runup flow unit of the tsunami deposit in Rikuzentakata City is the thickest, and therefore, it is reasonable to suggest that this unit may be correlated with the first inundating wave. With regard to successive waves, it is difficult to correlate these with flow units. Records from the GPS buoy indicate that the second and fourth waves were relatively high (approximately 2 m in height), whereas others were relatively small (less than 1.5 m in height). Hence, we tentatively correlate the second flooding flow unit to the second or the fourth wave, although future investigation using methods such as numerical simulation would seem necessary to confirm this correlation.

The analysis of sediment flux implies that the tsunami deposit in Rikuzentakata City included material not only from terrestrial erosion but also subaqueous erosion in Hirota Bay. The paleontological evidence clearly indicates that the sediment source of the tsunami deposit was at least partially from Hirota Bay. Bathymetric data indicate a water depth of 9 m. The total amount of sediment deposited on land was estimated to be $6.1 \times 10^5 \text{ m}^3$ (standard error: $1.5 \times 10^3 \text{ m}^3$). If all sediments were provided from the sandy spit eroded by the first tsunami wave ($3.5 \times 10^5 \text{ m}^2$), the average depth of erosional truncation would be approximately 1.7 m. Although the exact values should be determined by a future survey, this depth of erosion seems unlikely on the basis of visual observations. We infer that the erosional depth on the beach was less than 1 m (Fig. 4C and 4D), and that nearly half of the sediments were transported from the seafloor of Hirota Bay or from further offshore. Indeed, muddy sediments were widely distributed near the landward end of the inundation area, suggesting another sediment source of fine-grained sediments was available. Muddy sediments can be also sourced from the rice paddy fields, but erosion in the study area was limited to the coastal area

where rice fields were not present (Fig. 3). Trench examination suggested that the rice paddy fields were not markedly eroded (e.g. Fig. 6a), indicating a likely marine source for the fine-grained tsunami deposits.

6. Conclusion

The 2011 Tohoku-Oki tsunami deposited a large amount of sediments on land. A field survey at Rikuzentakata City, northeastern Japan, provided tsunami inundation characteristics for this region and a facies model of deposition on the bay-head deltas of estuarine systems.

(1) The tsunami deposit in Rikuzentakata City generally consisted of one- to four units that represent a discrete runup or backwash flow. Each unit was characterized by initial inverse grading (subunit I) and successive normal grading (subunit G), which correspond to the accelerating and decelerating stages of the flow, respectively. Between subunit I and G, an internal erosion surface often developed in response to the stage in which the flow reached maximum shear velocity, truncating the underlying inverse-graded subunit I. In case of the runup flow unit, the silty, fine-grained drapes (subunit S) overlaid the graded interval (subunit G). Features of multiple units with inverse-to-normal graded divisions are similar to the facies model for tsunami deposits in coastal plains, suggesting the general applicability of the model to multiple-bedded, terrestrial tsunami deposits.

(2) Correlation between the sedimentary structures and analysis of the grain fabric of the tsunami deposit revealed that the Tohoku-Oki tsunami inundated

Rikuzentakata City at least twice, and that flow velocity exceeded 2.4 m/s. Paleontological analysis of the sediment provenance and kriging estimation of the total volume of the tsunami deposits indicate that the sediments were derived not only from the eroded beach sands but also from the seafloor of Hirota Bay or more pelagic regions.

All the inferences obtained from the study of tsunami deposits in Rikuzentakata City can be used to refine future studies such as the development of numerical models. Although offshore tsunami hydrograph data are available, the complicated shape of Sanriku Coast affected the wave height and periodicity near the coast. Therefore, hydrodynamic numerical models of tsunamis are important for future disaster prevention planning, and data from tsunami deposits (such as the number of waves and minimum flow velocities of runup flows) provide important constraints for model verification. The amount and sources of sediments transported by the tsunami are also important factors for model verification. Morphodynamic models require sediment entrainment functions of bedload and suspended load for the calculation of landform developments, and numerous types of empirical functions have been proposed by various methods (e.g., Garcia and Parker, 1991). The choice of sediment entrainment functions should be tested by natural cases of complicated shorelines such as the tsunami deposits in Rikuzentakata City.

Acknowledgments

This survey was conducted as part of the research of The 2011 Tohoku Earthquake Tsunami Joint Survey Group (www.coastal.jp/tsunami2011). We gratefully

566 acknowledge their sincere contributions. We are grateful to Hitoshi Shibuya and Takuya
567 Matsuzaki for their help with field sampling and grain-size measurements at Kochi Core
568 Center. This study is dedicated to all those affected by the March 11, 2011 earthquake.
569

570 References

- 571 Abe, T., Goto, K., Sugawara, D., in press this issue Relationship between the maximum
572 extent of tsunami sand and the inundation limit of the 2011 Tohoku-Oki
573 tsunami on the Sendai Plain, Japan. *Sedimentary Geology*,
574 doi:10.1016/j.sedgeo.2012.05.004.
- 575 Asano, T., Matsumoto, C., Nagano, A., 2009. Functional Assessment on Coastal Forests
576 in Japan as Tsunami Barrier Facilities. *Journal of Hydraulic, Coastal and*
577 *Environmental Engineering (JSCE)* B2-65, 1311-1315. (in Japanese with
578 English abstract)
- 579 Benson, B.E., Grimm, K.A. & Clague, J.J. 1997. Tsunami deposits beneath tidal
580 marshes on northwestern Vancouver Island, British Columbia. *Quaternary*
581 *Research* 48, 192-204.
- 582 Brownlie, W.R., 1981. Prediction of flow depth and sediment discharge in open
583 channels. Report No. KH-R-43A, Keck Laboratory of Hydraulics and Water
584 Resources, California Institute of Technology, Pasadena, California.
- 585 Burgess, T.M., Webster, R., 1980a. Optimal interpolation and isarithmic mapping I. The
586 semi-variogram and punctual kriging. *European Journal of Soil Science* 31,
587 315-331.

- 588 Burgess, T.M., Webster, R., 1980b. Optimal interpolation and isarithmic mapping. II.
589 Block kriging. *European Journal of Soil Science* 31, 505–524.
- 590 Chagué-Goff, C., Andrew, A., Szczuciński, W., Goff, J., Nishimura, Y. in press this issue.
591 Geochemical signatures up to the maximum inundation of the 2011
592 Tohoku-oki tsunami - implications for the 869 AD Jōgan and other
593 palaeotsunamis. *Sedimentary Geology*. doi:[10.1016/j.sedgeo.2012.05.021](https://doi.org/10.1016/j.sedgeo.2012.05.021)
594
- 595 Chida, N., Matsumoto, H., Obara, S., 1984. Recent Alluvial Deposit and Holocene Sea
596 level Change on Rikuzentakata Coastal Plain, Northeast Japan. *Tohoku-Chiri*
597 36, 232-239. (in Japanese with English abstract).
598
- 599 Clague, J.J., Bobrowsky, P.T., Hutchinson, I., 2000. A review of geological records of
600 large tsunamis at Vancouver Island, British Columbia, and implications for
601 hazard. *Quaternary Science Reviews* 19, 849-863.
- 602 Dawson, S., Smith, D.E., 2000. The sedimentology of Middle Holocene tsunami facies
603 in northern Sutherland, Scotland, UK. *Marine Geology* 170, 69-79.
- 604 Dodd, N., Stoker, A.M., Calvete, D., Sriariyawat, A., 2008. On beach cusp formation.
605 *Journal of Fluid Mechanics* 597, 145-169.
- 606 Einstein, H.A., 1950. The Bedload Function for Bedload Transportation in Open
607 Channel Flows. Technical Bulletin No. 1026 , U.S.D.A., Soil Conservation
608 Service, 1–71.
- 609 Folk, R.L., 1966. A review of grain-size parameters. *Sedimentology* 6, 344–359.
- 610 Fujii, Y., Satake, K., Sakai, S., Shinohara, M., Kanazawa, T., 2011. Tsunami source of
611 the 2011 off the Pacific coast of Tohoku Earthquake. *Earth Planets Space* 63,

- 612 815–820.
- 613 Fujino, S., Naruse, H., Matsumoto, D., Sakakura, N., Suphawajruksakul, A.,
614 Jarupongsakul, T., 2010. Detailed measurements of thickness and grain size
615 of a widespread onshore tsunami deposit in Phang-nga Province,
616 southwestern Thailand. *Island Arc* 19, 389–398.
- 617 Fujiwara, O., 2007. Major contribution of tsunami deposit studies to Quaternary
618 Research. *The Quaternary Research (Daiyonki kenkyu)* 46, 293–302.
- 619 Garcia, M.H., 2008. Sediment Transport and Morphodynamics. In: Garcia M.H. (Eds.),
620 Sedimentation engineering: processes, management, modeling, and practice.
621 American Society of Civil Engineers, Virginia, USA, pp. 21-163.
- 622 García, M.H., Parker, G., 1991. Entrainment of Bed Sediment into Suspension. *Journal*
623 *of Hydraulic Engineering, ASCE* 117, 414–435.
- 624 Gelfenbaum, G., Jaffe, B., 2003. Erosion and sedimentation from the 17 July, 1998
625 Papua New Guinea Tsunami. *Pure and Applied Geophysics* 160, 1969-1999.
- 626 Goto, K., Chagué-Goff, C., Fujino, S., Goff, J., Jaffe, B., Nishimura, Y., Richmond, B.,
627 Sugawara, D., Szczuciński, W., Tappin, D.R., Witter, R., Yulianto, E., 2011.
628 New insights of tsunami hazard from the 2011 Tohoku-oki event. *Marine*
629 *Geology* 290, 46-50.
- 630 Goto, K., Chagué-Goff, C., Goff, J., Jaffe, B. (submitted this issue). The future of
631 tsunami research following the 2011 Tohoku-oki event. *Sedimentary*
632 *Geology*
- 633 Harrington, R.F., 1967. *Field Computation by Moment Methods*, 1st ed. The Macmillan
634 Co., New York.
- 635 Hiscott, R.N., 1994. Loss of capacity, not competence, as the fundamental process

- 636 governing deposition from turbidity currents. *Journal of Sedimentary*
637 *Research* 64, 209-214.
- 638 Ikeya, N., Cronin, T.M., 1993. Quantitative analysis of Ostracoda and water masses
639 around Japan: application to Pliocene and Pleistocene paleoceanography.
640 *Micropaleontology* 39, 263-281.
- 641 Keulegan, G.H., 1938. Laws of turbulent flow in open channels. *Journal National*
642 *Bureau of Standards, Research Paper* 1151, 707-741.
- 643 Kohsaka, H., 1998. Kriging and its Geographic Applications. *Bulletin of Nihon*
644 *University College of Humanities and Sciences* 34, 27-35.
- 645 Kon'no, E., 1961. Geological observations of the Sanriku coastal region damaged by
646 Tsunami due to the Chile Earthquake in 1960. *Contributions from the*
647 *Institute of Geology and Paleontology, Tohoku University* 52, 1-40. (in
648 Japanese with English abstract)
- 649 Moore, J.G., Moore, G.W., 1984. Deposit from a giant wave on the island of Lanai,
650 Hawaii. *Science* 226, 1312-1315.
- 651 Moore, A., Nishimura, Y., Gelfenbaum, G., Kamataki, T., Triyono, R., 2006.
652 Sedimentary deposits of the 26 December 2004 tsunami on the northwest
653 coast of Aceh, Indonesia. *Earth, Planets and Space* 58, 253-258.
- 654 Mori, N., Takahashi, T., Yasuda, T., Yanagisawa, H., 2011. Survey of 2011 Tohoku
655 earthquake tsunami inundation and run-up, *Geophysical Research Letters* 38,
656 doi:10.1029/2011GL049210.
- 657 Nanayama F., Shigeno, K., 2006. Inflow and outflow facies from the 1993 tsunami in
658 southwest Hokkaido. *Sedimentary Geology* 187, 139-158.
- 659 Nanayama, F., Satake, K., Furukawa, R., Shimokawa, K., Atwater, B.F., Shigeno, K. &

- 660 Yamaki, S., 2003. Unusually large earthquakes inferred from tsunami
661 deposits along the Kuril trench. *Nature* 424, 660–663.
- 662 Naruse, H., Fujino, S., Suphawajraksakul, A., Jarupongsakul, T., 2010. Features and
663 formation processes of multiple deposition layers from the 2004 Indian
664 Ocean Tsunami at Ban Nam Kem, southern Thailand. *Island Arc* 19,
665 399–411.
- 666 National Police Agency of Japan, 2012. [http://www.npa.go.jp/archive/keibi/biki/](http://www.npa.go.jp/archive/keibi/biki/higaijokyo_e.pdf)
667 [higaijokyo_e.pdf](http://www.npa.go.jp/archive/keibi/biki/higaijokyo_e.pdf).
- 668 Neill, C.R., Yalin. M.S., 1969. Qualitative definition of beginning of bed movement.
669 *Journal of the Hydraulics Division, ASCE* 95, 585–587.
- 670 Nelson, A.R., Sawai, Y., Jennings, A.E., Bradley, L.A., Gerson, L., Sherrod, B.L.,
671 Sabeau, J., Horton, B.P., 2008. Great-earthquake paleogeodesy and tsunamis
672 of the past 2000 years at Alsea Bay, central Oregon coast, USA. *Quaternary*
673 *Science Reviews* 27, 747–768.
- 674 Nettles, M., Ekstrom, G., Koss, H.C., 2011. Centroid-moment-tensor analysis of the
675 2011 off the Pacific coast of Tohoku Earthquake and its larger foreshocks
676 and aftershocks. *Earth, Planets and Space*, 63, 519–523.
- 677 Nishimura, Y., Miyaji, N., 1995. Tsunami deposits from the 1993 southwest Hokkaido
678 earthquake and the 1640 Hokkaido Komagatake eruption, northern Japan.
679 *Pure and Applied Geophysics* 144, 719–733.
- 680 Parker, G., 2005. ID morphodynamics of rivers and turbidity currents.
681 http://cee.uiuc.edu/people/parkerg/morphodynamics_e-book.htm.
- 682 Ramette, M.M., Heuzel, M.M., 1962. A study of pebble movement in the Rhone by
683 means of tracers. *La Houille Blanche, Special A.*, 389–398.

- 684 Shi, S., Dawson, A.G., Smith, D.E., 1995. Coastal sedimentation associated with the
685 December 12th 1992 Tsunami in Flores, Indonesia. *Pure and Applied*
686 *Geophysics* 144, 525–536.
- 687 Sperazza, M., Moore J.N., Hendrix M.S., 2004, High-Resolution Particle Size Analysis
688 of Naturally Occurring Very Fine-Grained Sediment Through Laser
689 Diffractometry. *Journal of Sedimentary Research* 74, 736-743.
- 690 Stimpson, I., 2011. Japan's Tohoku Earthquake and Tsunami. *Geology Today* 27, 96-98.
- 691 Switzer, A.D., Jones, B.G., 2008. Large-scale washover sedimentation in a freshwater
692 lagoon from the southeast Australian coast: sea-level change, tsunami or
693 exceptionally large storm? *The Holocene* 18, 787-803.
- 694 Takahashi, S., Toda, K., Kikuchi, Y., et al., 2011. Urgent Survey for 2011 Great East
695 Japan Earthquake and tsunami disaster in ports and coasts. Technical Note
696 of the Port and Airport Research Institute 1231, Port and Airport Research
697 Institute, Japan, Yokosuka, pp. 1-200.
- 698 Umitsu, M., 2006. Spatial distribution of tsunami flow and deposits of tsunami on the
699 Nam Khem Plain, southern Thailand. *Chikyu Monthly* 28, 546–552. (in
700 Japanese).
- 701 Van Rijn, L.C., 1982. Equivalent roughness of alluvial bed. *Journal of the Hydraulic*
702 *Division, ASCE* 108, 1215–1218.
- 703

Figure captions

Figure 1. Index maps of study area. A: Map of northeastern Japan showing epicenter of Tohoku Oki earthquake. B: Study area.

Figure 2. Locality maps of the study area. Estimation of inundation area is based on the Maps of the Area hit by the Tsunami of 11 March 2011, Northeast Japan by Tsunami Damage Mapping Team, Association of Japanese Geographers (http://danso.env.nagoya-u.ac.jp/20110311/map/index_e.html).

Figure 3. Airphotos of Rikuzentakata City provided by Geospatial Information Authority of Japan. A: Airphoto taken before the tsunami (2010). White arrows indicate Takata-Matsubara pine forest located on a wave-dominated spit. B: Airphoto taken after the tsunami (March 13th 2011). Yellow dashed lines indicate regions where erosional processes of the tsunami dominated. The photo shows Takata-Matsubara was eroded by the tsunami.

Figure 4. Photographs taken at Rikuzentakata City. A: Broken building in Rikuzentakata City. B: Poles flattened by the tsunami runup flow. C: Flute-like erosional features. Scale is 1 m. D: Collapsed coastal levee and Takata-Matsubara pine forest.

Figure 5. Photographs showing features of the tsunami deposit at Rikuzentakata City. A: Dunes formed by backwash flow. B: Garbage accumulated at the maximum extent of tsunami inundation area. C: Rice fields covered by tsunami deposits. D: Tsunami deposits in the parking area (Loc. 111).

Figure 6. Pictures of flow-parallel vertical sections of tsunami deposits in Rikuzentakata

726 City. Left is the seaward direction in all pictures. A: Wall of trench excavated
727 at Loc. 31. Boundary between the tsunami deposit and the original surface of
728 the rice field is smooth and shows no erosional feature. B: Tsunami deposit
729 peeled off from a trench wall onto cloth using polyurethane resin at Loc 14.
730 Scale bar is 5 cm. C: Tsunami deposit peeled off from a trench wall at Loc 93.
731 Cross lamination shows that the middle part of this deposit was formed by
732 backwash flow. Scale bar is 10 cm.

733 Figure 7. Directions of tsunami inundation flow measured from damaged artificial
734 objects such as bent power poles. Runup currents are dominant.

735 Figure 8. Thickness distributions of the tsunami deposit. A: Bubble plot of thickness of
736 the tsunami deposit at each sampling location. B: Kriging estimation of
737 spatial thickness distribution of the tsunami deposit in Rikuzentakata City.
738 White dashed line indicates distribution limit of sandy deposits. C: Standard
739 error of the result of the kriging estimation.

740 Figure 9. A typical example of the vertical variation of the tsunami deposit (Loc. 11E) in
741 mean grain-size. The deposit is characterized by inverse- to normal-graded
742 multiple units, although it lacks a silty subunit (subunit S). Bars indicate the
743 standard deviation of grain-size distribution at each interval.

744 Figure 10. Columnar sections showing cross profile of tsunami sand sheets in the main
745 city area of Rikuzentakata City. The locations of the sections are indicated in
746 Figure 2. The top of each columnar section corresponds to the local ground
747 surface. Reconstructions of paleo-flow directions are based on grain fabric
748 (Loc.19) and cross-laminations (Loc. 11W). Scale bars are 10 cm.

749 Figure 11 , Stratigraphic sections on flow-parallel transects showing a cross profile of

750 tsunami sand sheets in Otomo Area of Rikuzentakata City. The locations of
751 the two transects are indicated in Figure 2. The top of each section
752 corresponds to the local ground surface. Scale bars are 10 cm.

753 Figure 12. Rose diagrams showing results of grain fabric analysis of the tsunami deposit
754 in vertical sections. Imbrication angles of sand-sized grains at flow-parallel
755 vertical sections were examined and the runup and backwash flow units were
756 identified at each locality.

757 Figure 13. Mean grain-size distribution of the basal unit of the tsunami deposit. A:
758 Bubble plot of mean grain-size of the tsunami deposit at each sampling
759 location. B: Kriging estimation of spatial distribution of mean grain-size. C:
760 Standard error of the kriging estimation results.

761 Figure 14 Bubble plot of the critical flow velocity of gravels. The runup or backwash
762 flow of the tsunami in Rikuzentakata City must exceed these values at each
763 sampling point.

764 Figure 15. A: Map of Japan showing locations of the study area and the reference site
765 OK28. B: Scanning electron microscope images of characteristic species
766 recovered from sample c: (1) *Bicornucythere bisanensis* (2) *Nipponocythere*
767 *bicarinata*; (3) *Spinileberis quadriaculeata*; (4) *Cytheromorpha acupunctata*.

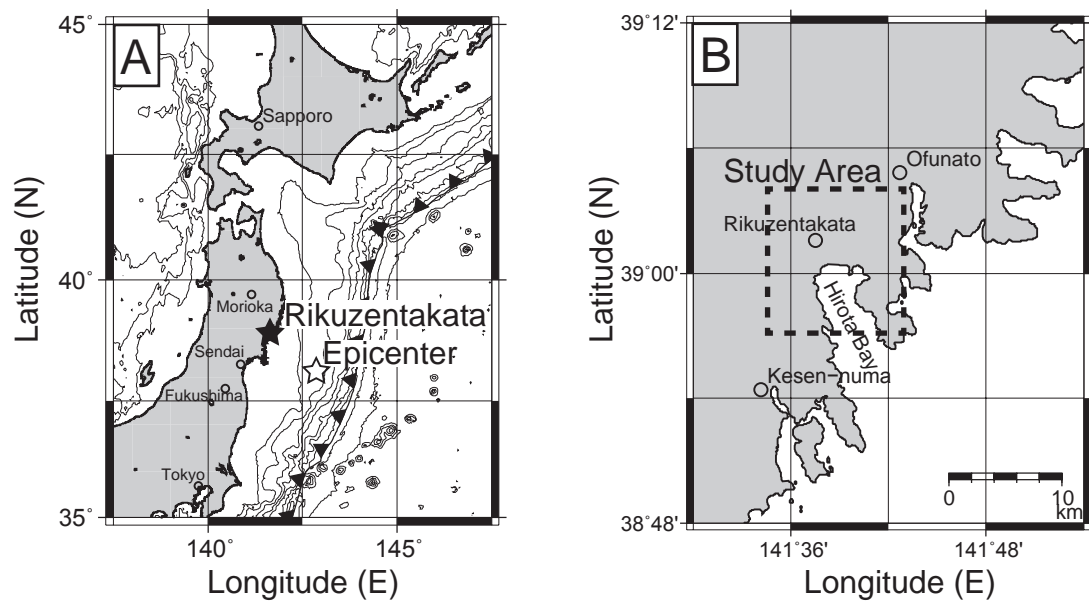
768
769 Figure 16 Schematic model of the formation process of multiple-bedded tsunami
770 deposits. A: Typical variation of the tsunami sequence that was frequently
771 observed in Rikuzentakata City. Subunits I, G and S indicate inverse-graded,
772 graded, and silty subunits. The ideal tsunami sequence formed by a single
773 wave is composed of two units, consisting of subunits I-G-S-I-G. At the

774 turnover stage from backwash to run-up, there is no ponding of stagnant
775 water on land so that a thick, silty subunit (subunit S) is not found at the top
776 of the backwash depositional unit. Inverse-graded subunits of runup flow
777 units and 1st backwash-flow unit were lost due to erosion. B: Schematic
778 formative process of the inverse- to normal-graded bedding in the tsunami
779 deposit. Flow conditions for processes 1-3 are shown in Figure 16A. An
780 internal erosion surfaces (IES) often develops between the inverse and normal
781 graded subunits.

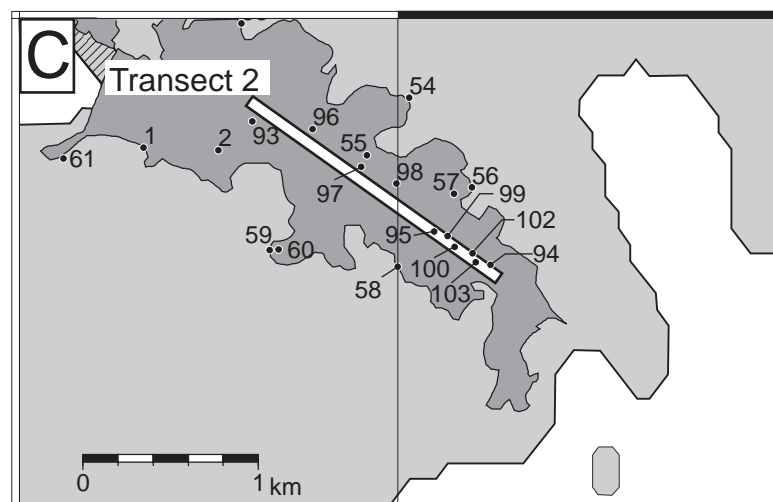
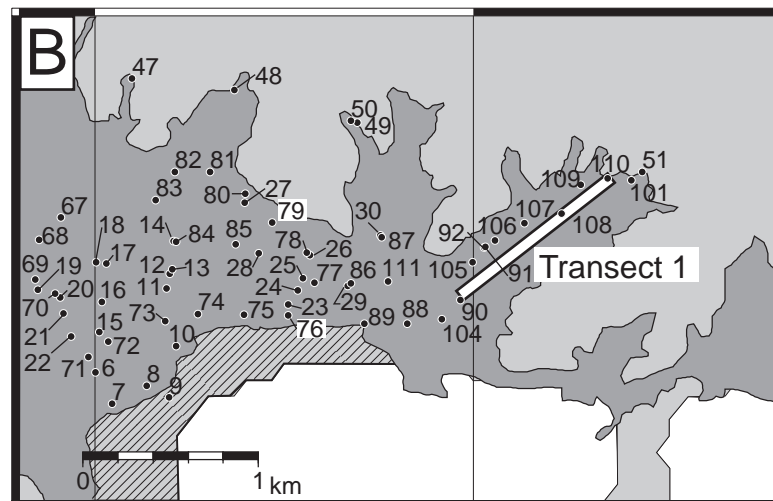
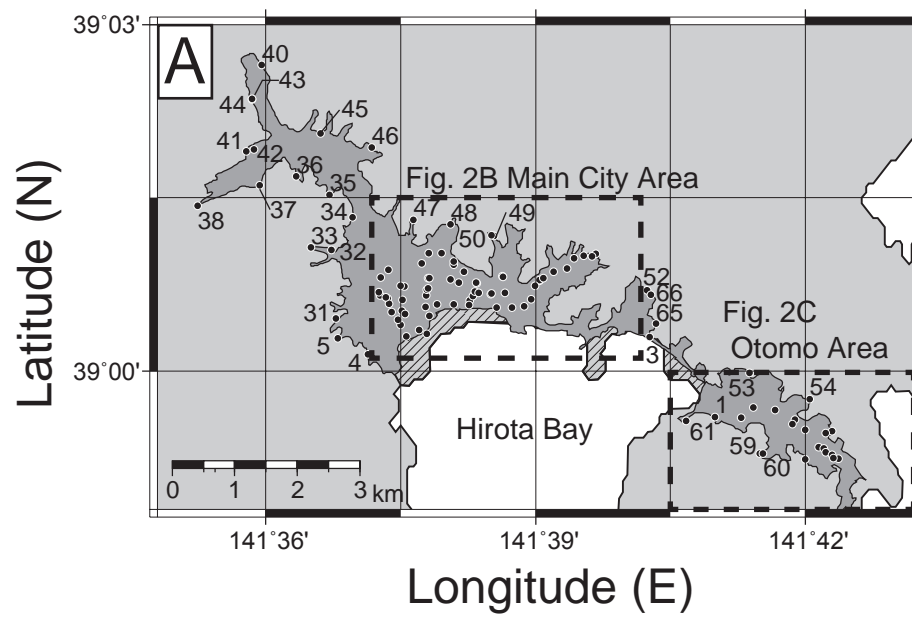
782

783 Table 1. Ostracods species observed in the tsunami deposits.

784 Table 2. Result of grain-size analysis by laser granulometer. All grain-size values are
785 shown in phi scale. Max. G is the maximum grain size.

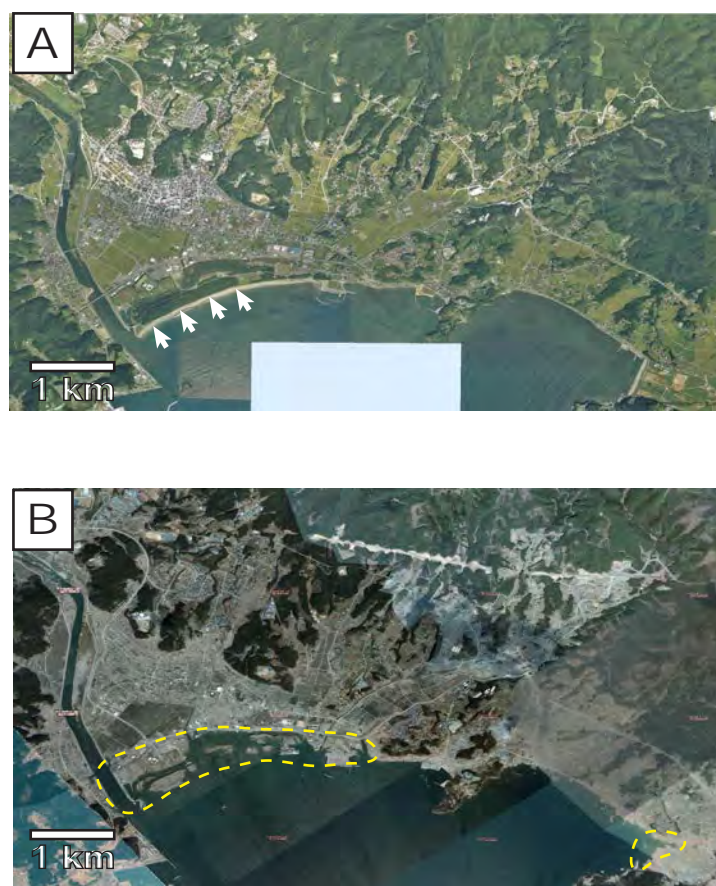


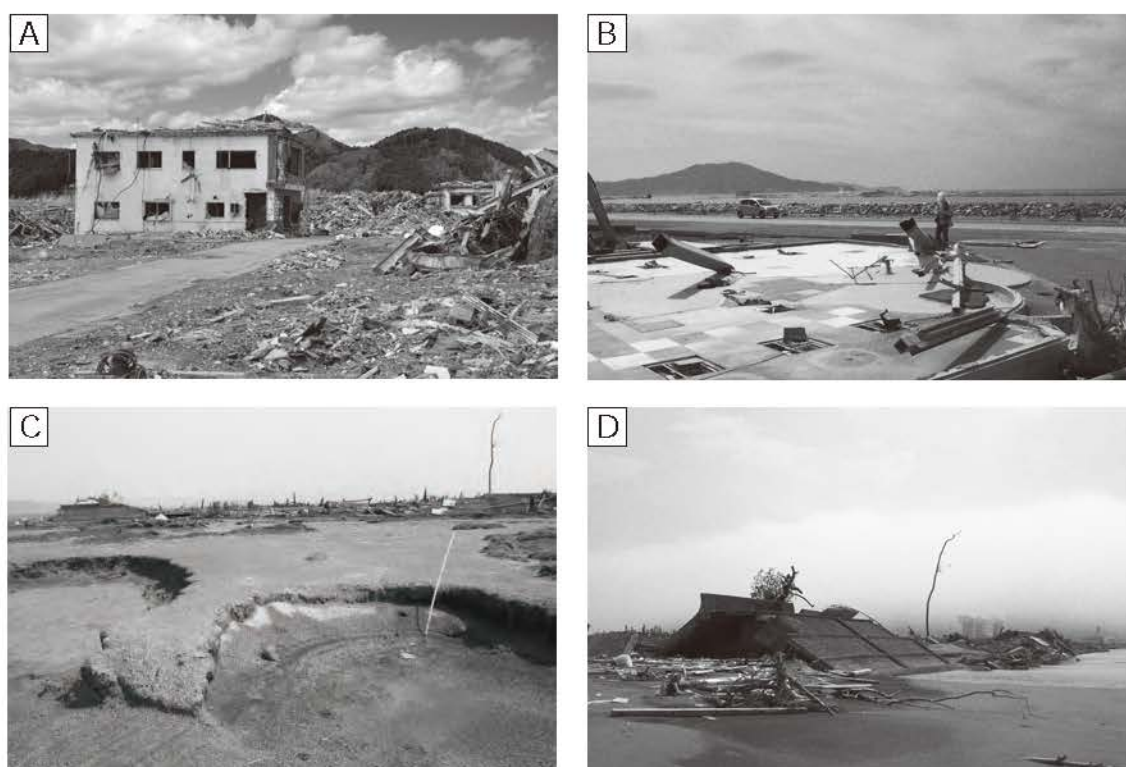
Naruse et al. Fig. 1



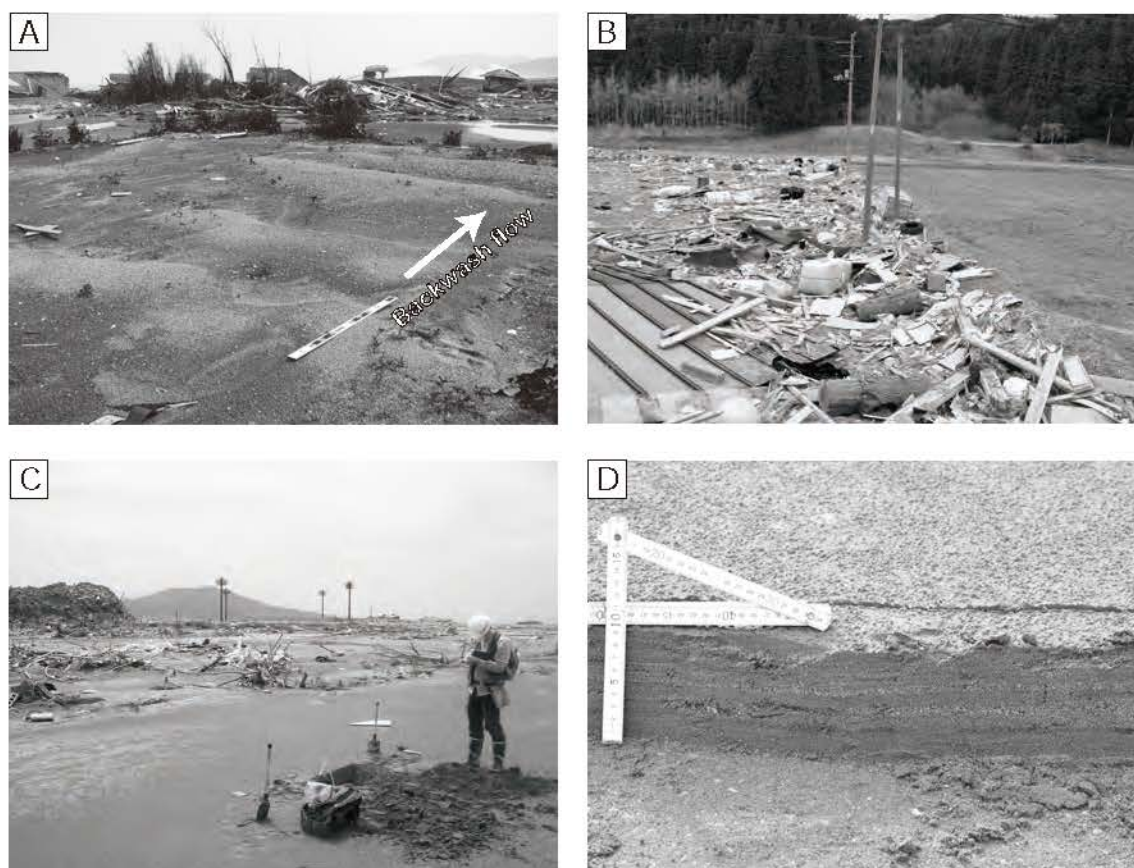
■ Inundation area ▨ Eroded area

Naruse et al. Fig. 2



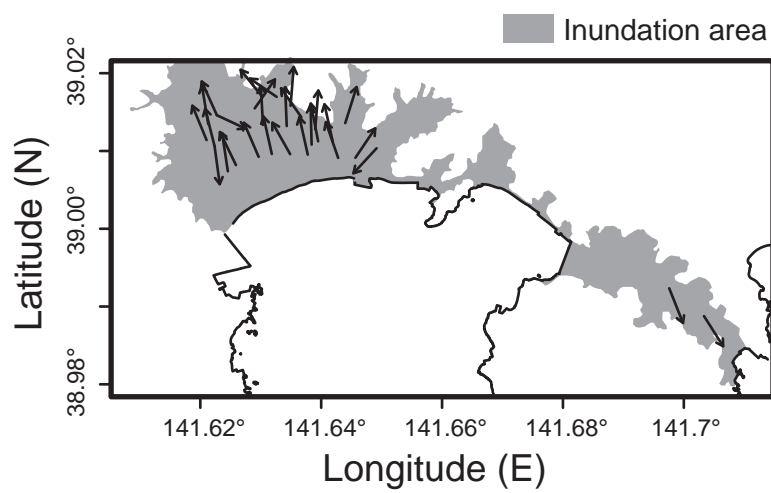


Naruse et al. Fig. 4

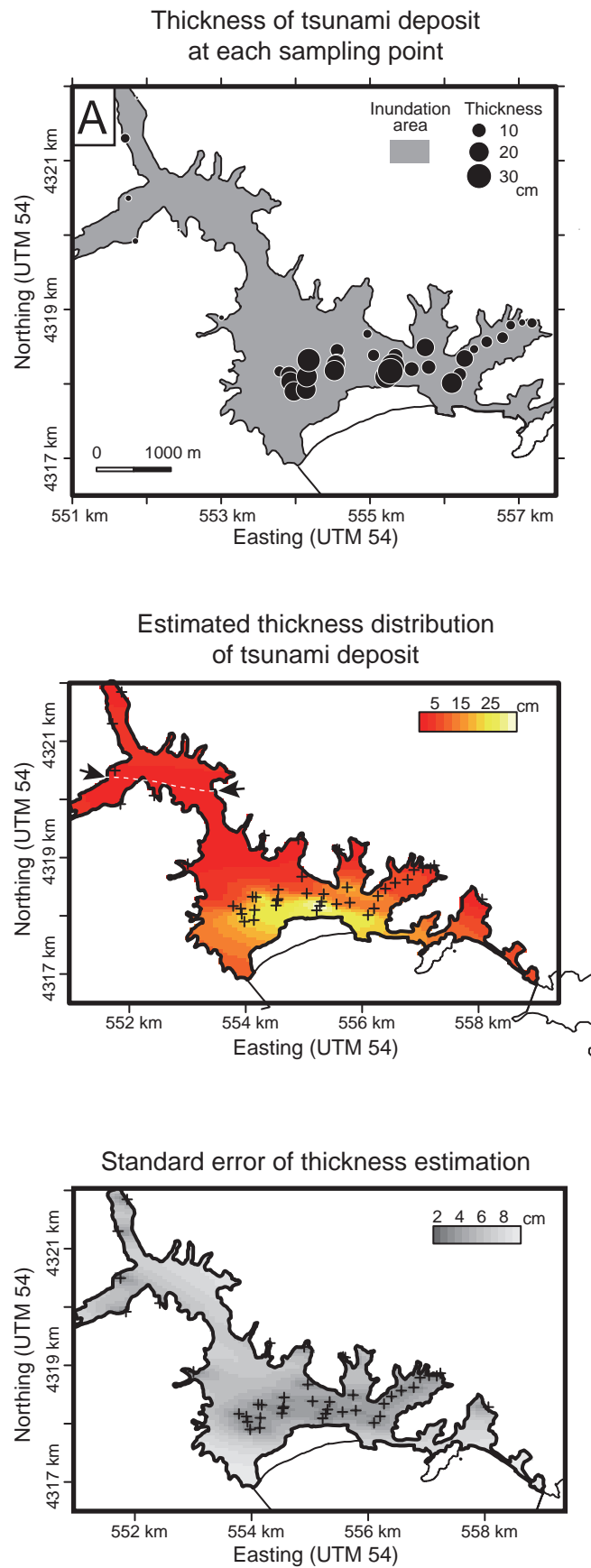


Naruse et al. Fig. 5

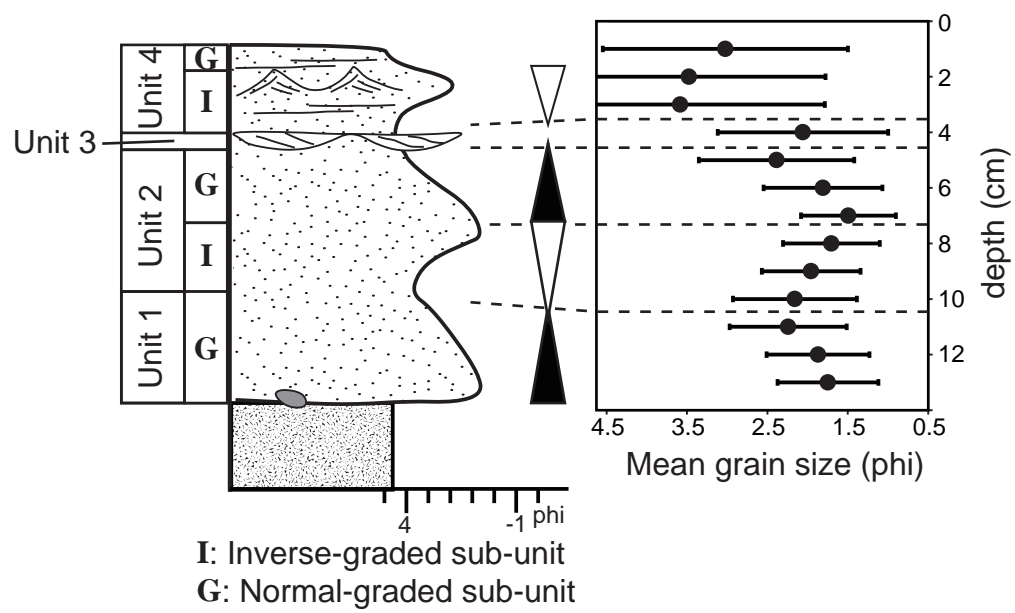




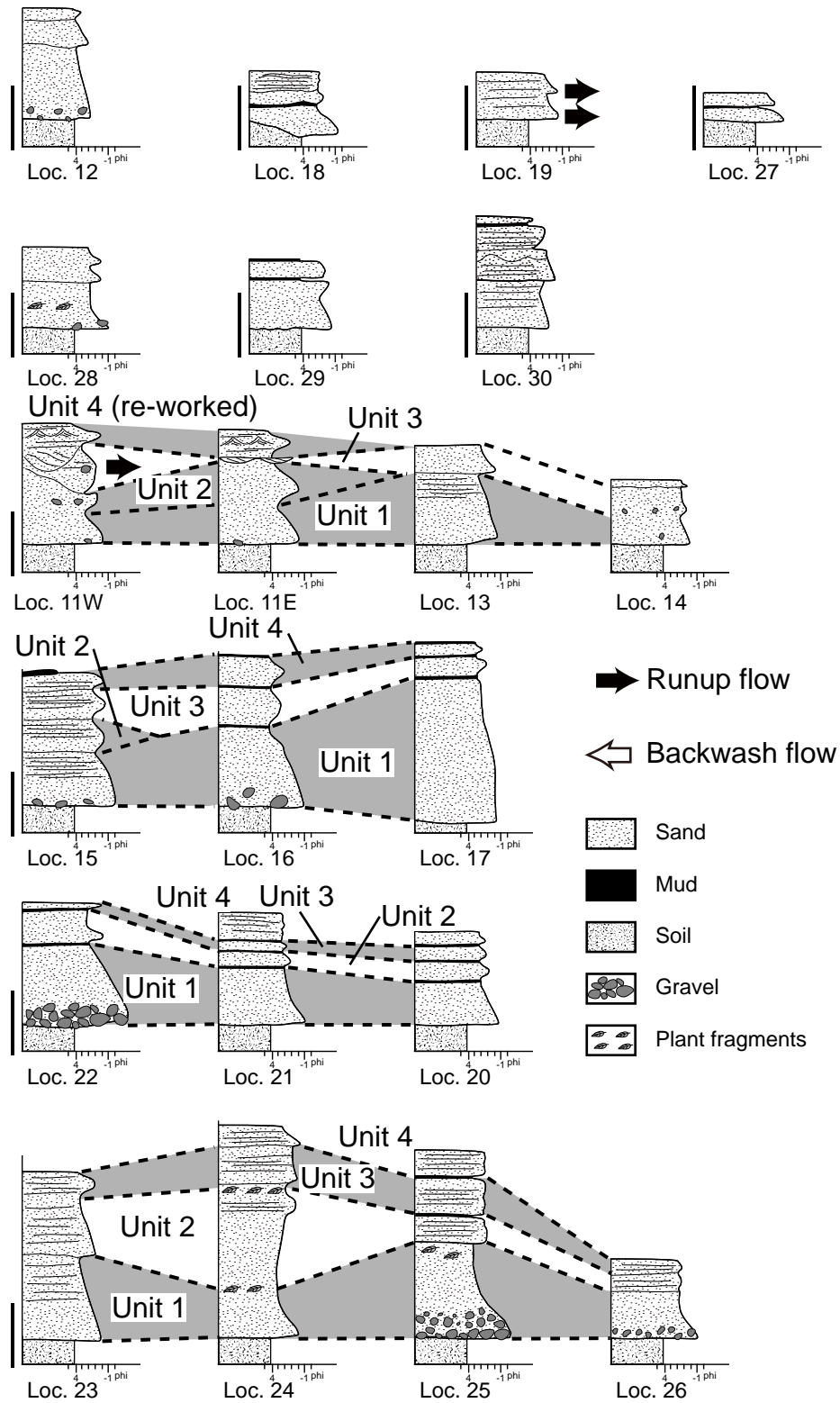
Naruse et al. Fig. 7



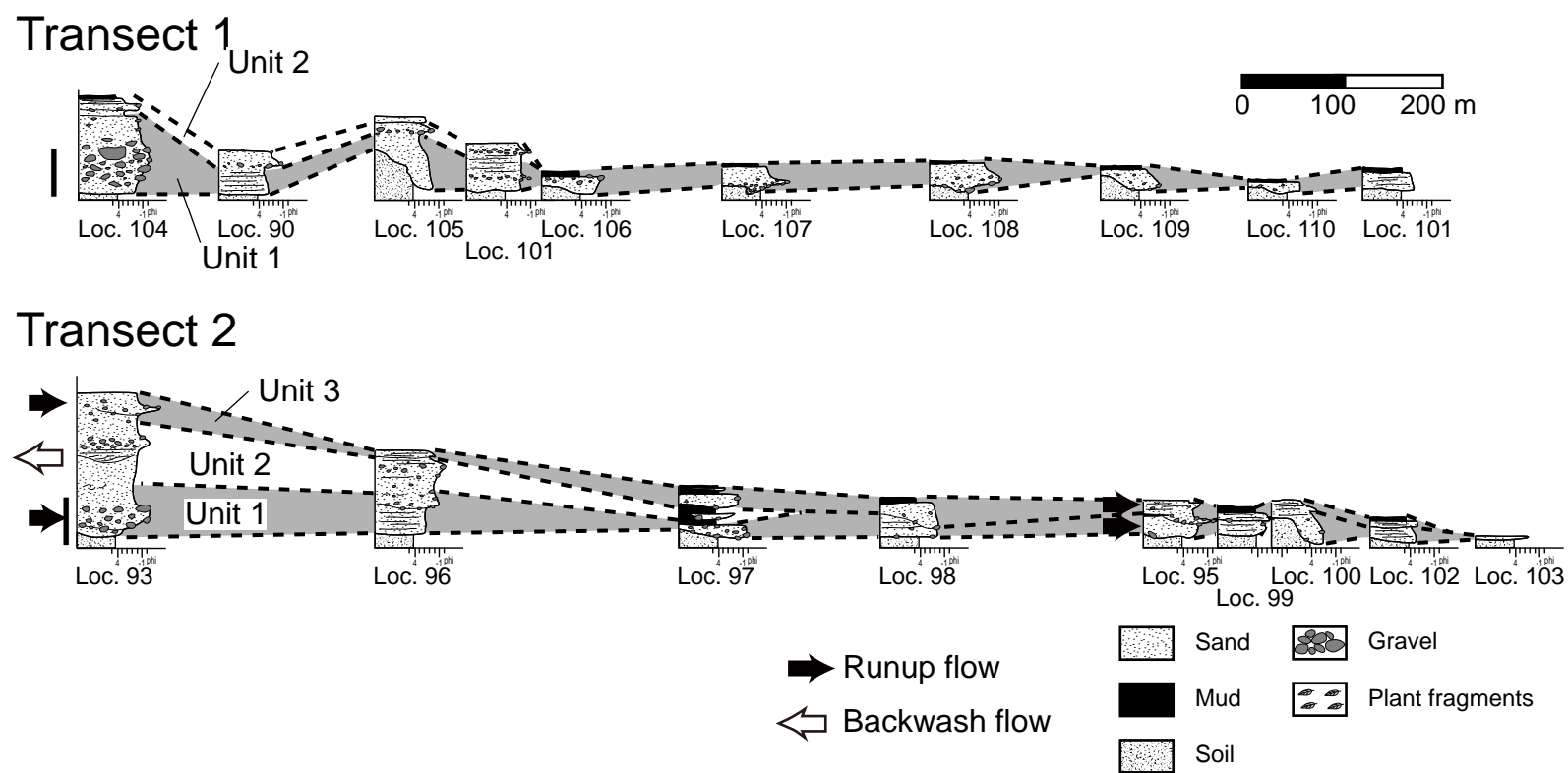
Naruse et al. Fig. 8



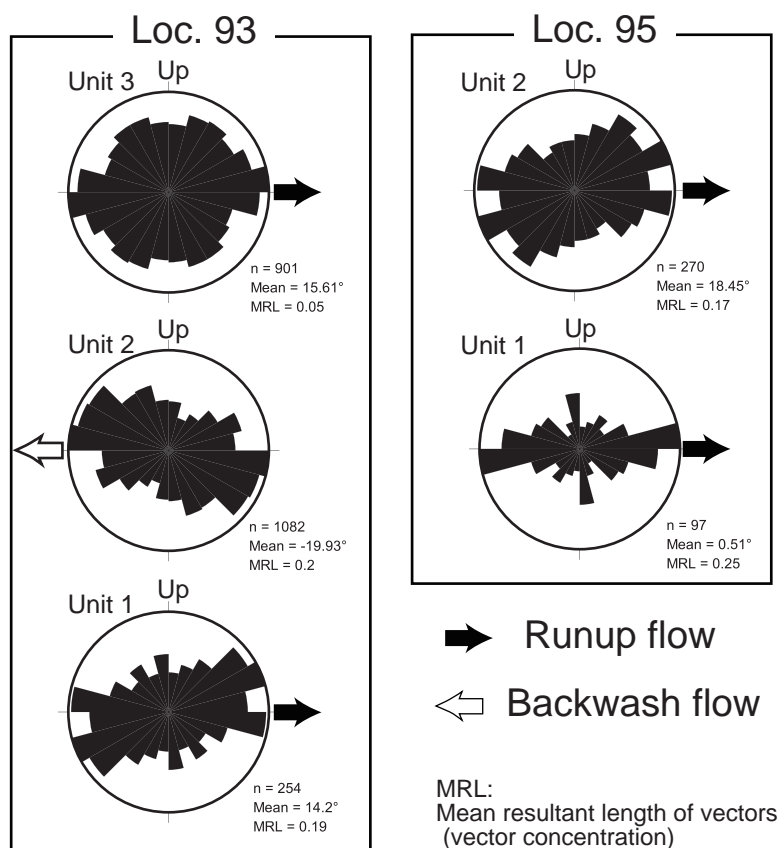
Naruse et al. Fig. 9

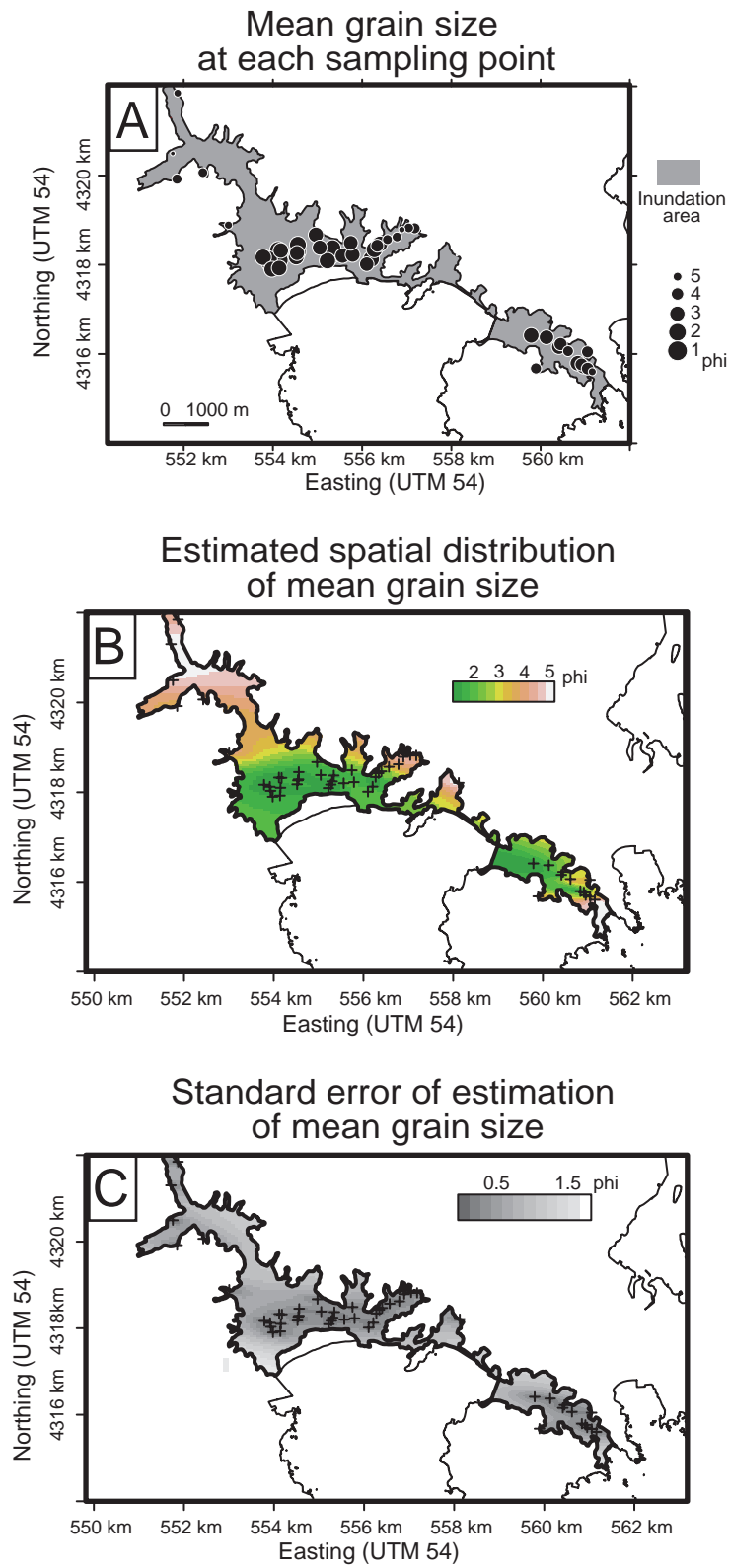


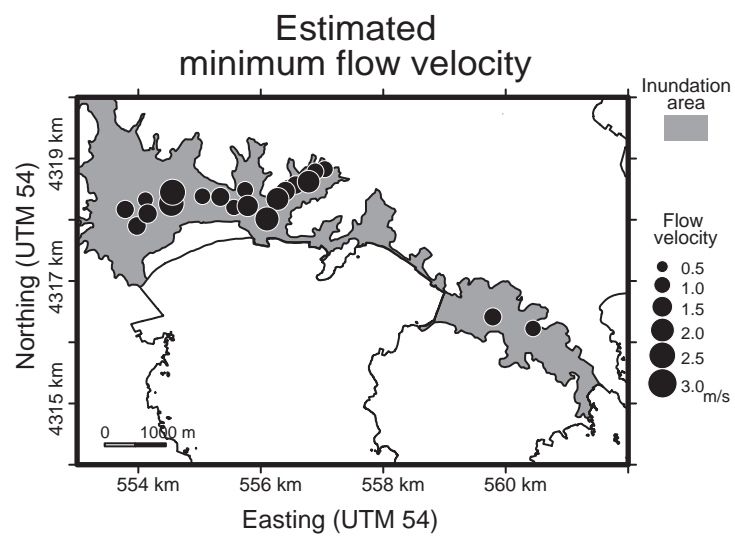
Naruse et al. Fig. 10

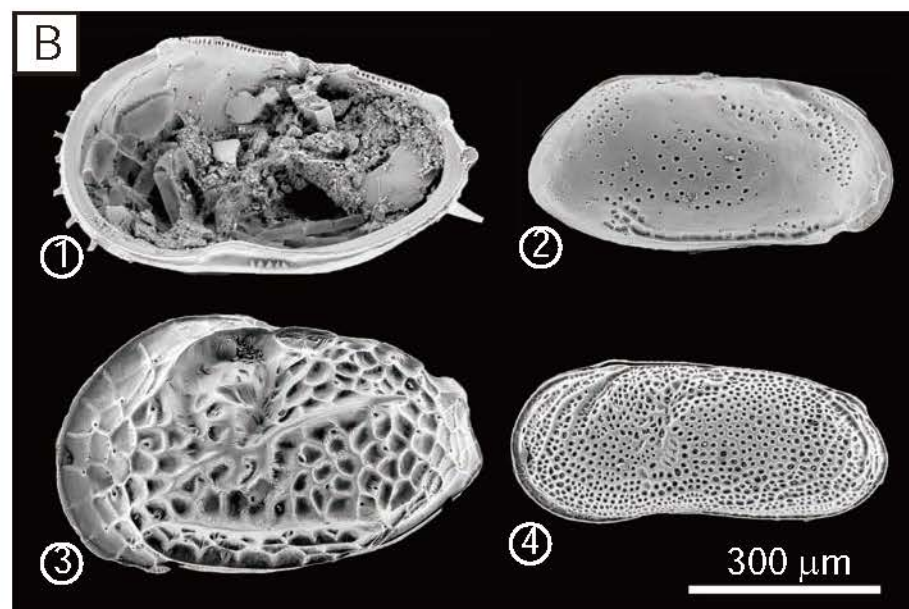
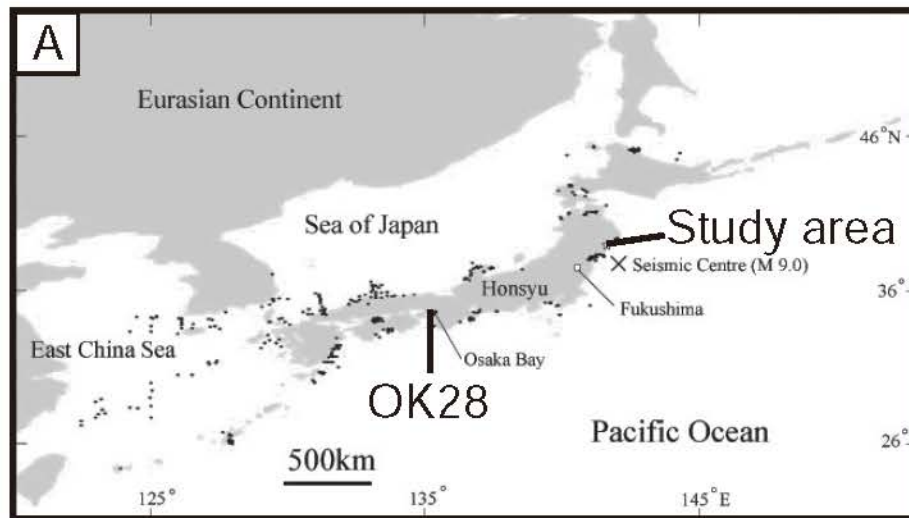


Naruse et al. Fig. 11.

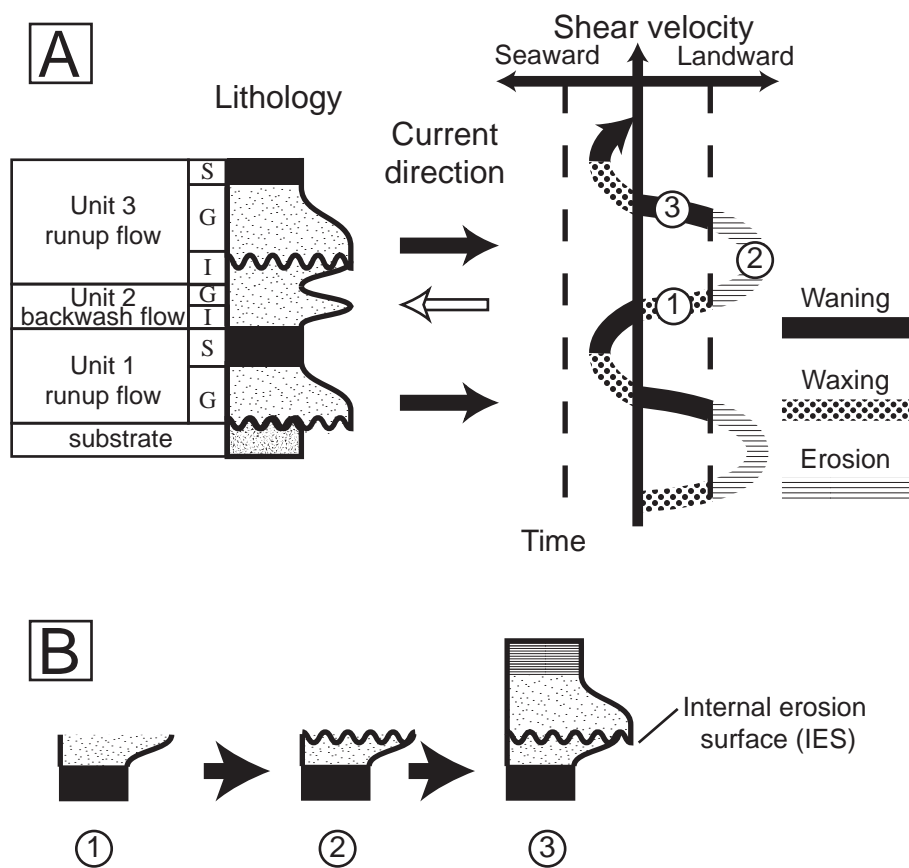








Naruse et al. Fig. 15



<i>Angulicytherura miii</i>	1				
<i>Aurila corniculata</i>			14	11	
<i>Bicornucythere bisanensis</i>			36	17	
<i>Bythoceratina hanaii</i>			2		
<i>Bythoceratina hanaii</i>			2		
<i>Callistocythere japonica</i>			1		
<i>Callistocythere undulatifacialis</i>			2		
<i>Coquimba ishizakii</i>			3		
<i>Cornucoquimba tosaensis</i>			3		1
<i>Cytherois nakanoumiensis</i>			2		
<i>Cytheromorpha acupunctata</i>			6	3	
<i>Hemicytherura kajiyamai</i>			3	1	
<i>Howeina leptocytheroidea</i>			3	1	
<i>Kobayashiina donghaiensis</i>			2		
<i>Loxoconcha epeterseni</i>			1		1
<i>Loxoconcha japonica</i>			2		
<i>Loxoconcha ozawai</i>			2		
<i>Loxoconcha uranouchiensis</i>			3	1	
<i>Neonesidea oligodentata</i>			9	2	
<i>Nipponocythere bicarinata</i>			8	1	
<i>Parakrithella pseudadonta</i>			1		
<i>Pistocythereis bradyformis</i>			2		
<i>Pontocythere subjaponica</i>	1		6	2	4
<i>Schizocythere kishinouyei</i>				2	
<i>Semicytherura miurensis</i>			5		
<i>Spinileberis quadriaculeata</i>			16	16	
<i>Xestoleberis hanaii</i>			19	3	1
<i>Xestoleberis sagamiensis</i>			1		
<i>Xestoleberis setouchiensis</i>				2	
Total	1	1	157	63	7



30	Total	97.0	3.0	2.04	0.94	1.82	10.09	3.01	1.94	1.01	
	京都大学	96.7	3.3	2.23	0.96	1.69	9.17	3.24	2.00	1.00	
	KYOTO UNIVERSITY	97.6	2.4	1.85	0.90	1.90	10.94	2.77	1.91	1.00	
	Unit 3	96.7	3.3	2.03	0.98	1.90	10.20	3.02	1.92	0.99	
32		35.3	64.7	4.78	1.80	0.02	2.73	7.22	4.71	2.45	
36		59.3	40.7	3.93	1.91	0.59	2.78	6.81	3.52	1.82	
37		64.2	35.8	3.81	1.73	0.89	3.60	6.54	3.46	2.00	
40		53.1	46.9	4.23	2.07	0.35	2.50	7.33	3.84	1.82	
41		36.4	63.6	4.70	1.85	-0.03	2.76	7.18	4.64	2.43	
43		31.1	68.9	5.01	1.89	-0.11	2.42	7.49	5.08	2.51	
54		81.7	18.3	2.76	1.67	0.85	3.97	4.89	2.60	0.78	-5.09
56		75.6	24.4	3.16	1.90	1.06	3.55	6.24	2.70	1.17	
59		66.3	33.7	3.42	1.98	0.72	2.65	6.42	2.89	1.22	
66		30.6	69.4	4.96	1.98	-0.25	2.40	7.44	5.16	2.08	
90	Total	90.5	9.5	2.02	1.47	1.64	6.46	3.90	1.70	0.58	
	Unit 1	92.7	7.3	1.88	1.49	1.56	6.77	3.57	1.64	0.37	
	Unit 2	95.3	4.7	1.50	1.30	2.19	9.96	2.69	1.28	0.26	
91	Total	89.8	10.2	2.08	1.48	1.61	6.13	4.05	1.74	0.64	
	Unit 1	84.5	15.5	2.86	1.60	1.56	5.40	5.27	2.49	1.32	-5.61
	Unit 2	81.6	18.4	3.17	1.39	1.31	5.70	4.71	2.97	1.71	
93	Total	91.7	8.3	1.80	1.46	1.64	6.35	3.69	1.46	0.38	
	Unit 1	90.7	9.3	1.89	1.50	1.58	5.92	3.87	1.52	0.43	-5.73
	Unit 2	93.7	6.3	1.67	1.37	1.72	7.08	3.34	1.37	0.31	
	Unit 3	92.5	7.5	1.64	1.43	1.81	7.02	3.49	1.31	0.29	
94		53.1	46.9	4.18	1.75	0.58	2.79	6.78	3.86	2.16	
95		90.0	10.0	1.84	1.54	1.80	6.42	3.98	1.44	0.44	
96	Total	85.1	14.9	2.45	1.54	1.29	5.31	4.40	2.18	0.79	
	Unit 1	91.1	8.9	2.22	1.35	1.71	6.92	3.80	1.95	0.88	
	Unit 2	92.6	7.4	1.97	1.36	1.38	5.75	3.64	1.71	0.53	
97	Total	76.7	23.3	2.84	1.77	0.86	3.65	5.26	2.57	0.80	
	Unit 1	87.2	12.8	2.15	1.65	1.27	4.71	4.35	1.76	0.45	
	Unit 2	76.1	23.9	2.98	1.71	0.71	3.50	5.20	2.85	0.89	
98		64.1	35.9	3.48	2.07	0.60	2.55	6.58	3.11	1.06	
99	Total	68.6	31.4	3.29	1.83	0.81	3.21	5.98	2.90	1.25	
	Unit 1	78.6	21.4	2.77	1.74	1.07	3.73	5.37	2.32	0.94	
	Unit 2	58.5	41.5	3.73	1.82	0.49	2.59	6.28	3.53	1.50	
100	Total	67.6	32.4	3.36	1.86	0.79	3.17	6.12	2.95	1.30	
	Unit 1	80.3	19.7	2.72	1.71	1.19	4.07	5.29	2.27	0.98	
	Unit 2	65.1	34.9	3.61	1.82	0.75	2.90	6.33	3.21	1.56	
101		59.3	40.7	3.72	1.99	0.52	2.62	6.63	3.33	1.40	
102	Total	83.0	17.0	2.67	1.58	1.30	5.55	4.48	2.44	0.96	
	Unit 1	78.0	22.0	2.93	1.70	1.00	3.76	5.41	2.58	1.08	
	Unit 2	56.7	43.3	3.83	1.77	0.42	2.78	6.29	3.67	1.61	
104	Total	86.3	13.7	2.52	1.55	1.42	6.08	4.18	2.30	0.88	
	Unit 1	91.6	8.4	2.30	1.45	1.61	6.85	3.66	2.11	0.80	
	Unit 2	75.2	24.8	2.81	2.06	0.83	3.02	6.01	2.34	0.54	
	Unit 3	51.8	48.2	4.13	1.86	0.42	2.56	6.73	3.93	1.83	-8.05
105	Total	90.5	9.5	1.61	1.68	1.65	6.03	3.99	1.20	0.03	
	Unit 1	88.7	11.3	1.52	1.78	1.77	5.89	4.30	1.02	-0.04	-7.57
	Unit 2	95.5	4.5	1.65	1.40	1.48	6.78	3.15	1.46	0.14	
	Unit 3	90.8	9.2	2.00	1.60	1.29	5.32	3.84	1.78	0.25	
106	Total	78.5	21.5	2.43	1.91	1.27	4.34	5.39	1.91	0.54	
	Unit 1	86.6	13.4	1.86	1.89	1.56	5.01	4.84	1.28	0.15	-6.38
	Unit 2	54.0	46.0	4.13	1.99	0.42	2.36	7.05	3.78	1.71	
107		59.0	41.0	3.74	1.99	0.51	2.39	6.61	3.37	1.39	-5.95
108		55.8	44.2	3.78	2.41	0.30	1.88	7.18	3.40	0.84	-7.54
109		33.5	66.5	4.87	1.89	-0.09	2.36	7.33	4.95	2.24	-5.48
110		59.9	40.1	3.80	1.94	0.60	2.55	6.69	3.41	1.54	-5.32
111	Total	93.1	6.9	2.41	1.19	1.59	7.93	3.63	2.27	1.15	
	Unit 1	97.0	3.0	2.23	1.00	1.57	8.86	3.25	2.15	1.12	-7.01
	Unit 2	91.2	8.8	2.59	1.29	1.77	7.96	3.83	2.42	1.29	
	Unit 3	88.5	11.5	2.54	1.40	1.43	6.36	4.06	2.34	1.07	